

Photonic Integrated Circuit-Based FMCW Coherent LiDAR

Aude Martin, Delphin Dodane, Luc Leviandier, Daniel Dolfi, *Senior Member, IEEE*, Alan Naughton, Peter O'Brien, Thijs Spuessens, Roel Baets , Guy Lepage, Peter Verheyen, Peter De Heyn, Philippe Absil, Patrick Feneyrou, and Jérôme Bourderionnet 

(Invited Paper)

Abstract—We present the demonstration of an integrated frequency modulated continuous wave LiDAR on a silicon platform. The waveform calibration, the scanning system, and the balanced detectors are implemented on a chip. Detection and ranging of a moving hard target at upto 60 m with less than 5 mW of output power is demonstrated in this paper.

Index Terms—Coherent LiDAR, frequency modulated continuous wave LiDAR, laser range finder, optical sensing and sensors, photonic integrated circuits.

I. INTRODUCTION

IN ORDER to further support the development of unmanned vehicles, compact eye-safe detection and ranging systems capable of 3D-mapping are required. Compared to RADAR technologies, detection and ranging using light, also called LiDAR, enables to get much better axial resolution thanks to the directivity and focusing of the optical beam during its propagation. LiDAR systems, which also have a wide range of applications depending on the implementation, are hence quite sought out.

A first distinction has to be made between LiDAR systems based on the optical measurement type. Pulsed based LiDARs carry out telemetry measuring the *time of flight* as already demonstrated for topography measurements, contactless surface analysis and forest controls. *Doppler effect* is also investigated

for accurate measurements of the speed of hard or diffuse targets. For instance, the speed of vortices on airport runways is retrieved from the measurement of the frequency offset between the transmitted and received signals of long pulsed signals [1]. Analysis of other parameters (e.g., *power spectral density of backscattered light*) makes it possible to measure densities and gas temperatures for meteorological and environmental studies [2]. Here we implemented on-chip the architecture of a frequency modulated continuous wave coherent LiDAR, already demonstrated with fibered devices at very long ranges [3], that exploits both the *time of flight* and *Doppler effect*. The optical frequency modulation of the continuous wave source enables to measure simultaneously and independently the range and speed of a target with a resolution limited by the coherence time of the source and the bandwidth covered by the frequency waveform. Moreover the ambiguity range of such a LiDAR is defined by the period of the frequency chirp and may be tailored at will to produce multi-function LiDARs [4].

Another key implementation difference between LiDARs is the detection system. Direct detection schemes analyze the backscattered signal power and hence impose a strong impediment to real life applications as they are sensitive to solar glare and require high levels of optical output power. However, the development of single photon avalanche diodes (SPAD) challenges this assumption and has enabled 3D-imaging at up to 10 km range [5]. With a coherent detection as implemented here, pW signals can be detected thanks to the beating of the backscattered light with a local oscillator and the system stays insensitive to sun light and immune to jamming with relatively low-cost COTS detectors.

Therefore, as high peak powers need to be handled with care with Photonic integrated circuits (PIC), coherent FMCW is considered a valuable option for the implementation of a LiDAR on chip. Through monolithic integration, PICs are able to provide both electronic and optical devices on the same chip as well as thermal and mechanical stability. Besides the silicon technology is getting mature thanks to foundries, which supply parallel manufacturing paving the way for mass production. These developments, motivated by coherent communication applications, may now benefit coherent imaging. For instance, frequency combs that have turned into a burning topic for integrated photonic telecommunications are also interesting building blocks for high

Manuscript received February 21, 2018; revised May 16, 2018; accepted May 21, 2018. Date of publication May 28, 2018; date of current version August 30, 2018. This work was supported by the European Unions Seventh Programme for research, technological development, and demonstration under Grant 318178 - PLAT4M. (Corresponding author: Jérôme Bourderionnet.)

A. Martin, D. Dodane, L. Leviandier, D. Dolfi, P. Feneyrou, and J. Bourderionnet are with the Thales Research and Technology, Palaiseau 91120, France (e-mail: aude.martin@thalesgroup.com; delphin.dodane@thalesgroup.com; luc.leviandier@thalesgroup.com; daniel.dolfi@thalesgroup.com; patrick.feneyrou@thalesgroup.com; jerome.bourderionnet@thalesgroup.com).

A. Naughton and P. O'Brien are with the Tyndall National Institute, University College Cork, Cork T12 K8AF, Ireland (e-mail: alan.naughton@tyndall.ie; peter.obrien@tyndall.ie).

T. Spuessens and R. Baets are with the Ghent University-IMEC, Ghent 9000, Belgium (e-mail: Thijs.Spuessens@UGent.be; Roel.Baets@UGent.be).

G. Lepage, P. Verheyen, P. De Heyn, and P. Absil are with the IMEC-Leuven, Leuven 3001, Belgium (e-mail: guy.lepage@imec.be; peter.verheyen@imec.be; peter.deheyn@imec.be; philippe.absil@imec.be).

Color versions of one or more of the figures in this paper are available online at <http://ieeexplore.ieee.org>.

Digital Object Identifier 10.1109/JLT.2018.2840223

resolution and ultra-fast range finding [6], [7]. However, such on-chip demonstrations were limited to ranging of up to a few millimeters [8], [9].

The architecture of a 3D FMCW LiDAR requires a balanced detection, a frequency shifting method and a scanning system. On-chip, either one or two of these building blocks have been used simultaneously in a ranging experiment. In [10], the detection, implemented on-chip with an array of coherent pixels allowed the detection of a non-moving object at a maximum range of 50 cm with 120 mW of output power. In another demonstration [11], a laser was modulated using an electronic-photonic integrated circuit phase-locked loop to map a non moving object at up to 1.4 m with a high resolution. Lately, solid state beam steering based on optical phased arrays were also implemented with a balanced detection [12]. Limited by the input power on the silicon chip, the maximum output power of 1 mW enabled to detect a target at up to 1.5 m with a velocity of 300 mm/s.

Here, we demonstrate a coherent LiDAR where the calibration of the laser modulation waveform, the detection system and the switching between 8 channels are present on a single CMOS-compatible chip. Light is coupled out via grating couplers into fibers and spatial scanning is obtained with collimation lenses pointing in 8 different directions. We demonstrate also for the first time to our knowledge the detection and ranging of a moving hard target at up to 60 m with a LiDAR on-chip and scanning of a target at 8 m with 5 mW of optical power. Interestingly, these measurements were not limited by the optical power as we could couple out up to 20 mW, but rather by the coherence length of our DFB laser.

II. PRINCIPLE OF OPERATION AND WAVEFORM CALIBRATION

The output chirped beam is backscattered on a target at distance d moving with a radial speed v . The signal is then collected and combined with an undelayed laser output, the local oscillator. A Fourier transform is applied on the mixed signal and beat frequencies are obtained, ν_+ and ν_- . The range and speed are then obtained as :

$$d = \frac{c}{4\alpha}(\nu_- - \nu_+) \quad (1)$$

$$v = \frac{\lambda}{4}(\nu_- + \nu_+) \quad . \quad (2)$$

The signal processing of an alike but fully fibered LiDAR has been detailed elsewhere [4] and range finding as well as anemometry measurements have been performed [3]. The frequency sweep of the laser source is critical for such systems as the resolution is linked to the bandwidth of the modulation (B) as $\Delta z = c/2B$. However, sources with a long coherence length, favorable for long distance ranging, have a limited frequency sweep bandwidth and fast and large frequency sweep of lasers have a detrimental effect on the coherence length of a swept source [13].

For intermediate distance measurement, in the range of a few tens of meters, a DFB laser is able to demonstrate frequency modulation over large bandwidth and has a linewidth which can be as low as a few hundreds of kHz. Recently, commercially available array of DFB lasers has been used and the individual bandwidth of up to 12 DFB lasers was combined [14]. This

approach emulates a strongly modulated DFB laser with a lower frequency noise compared to a single DFB source with similar modulation.

In the experiment presented here, the optical frequency of a DFB laser (Gooch and Housego AA1401 series) is modulated with four different slopes $\pm\alpha$, $\pm\beta$ with $\alpha = 14 \text{ MHz}/\mu\text{s}$ and $\beta = 16 \text{ MHz}/\mu\text{s}$. The Fourier transforms of the beating signal are computed on temporal segments of $33 \mu\text{s}$ which corresponds to a frequency bandwidth B of 525 MHz. The range resolution of our LiDAR is limited by the modulation bandwidth of the laser according to $\Delta d_{res} = c/2B = 28 \text{ cm}$. The repetition rate of the waveform is 1.9 kHz. The calibration of the waveform is performed on the fly using a delay line interferometer in order to compensate for thermal drifts during the measurement, as it affects the precision of the ranging. Indeed any deviation of the optical length difference between both arms of the calibration interferometer leads to an inaccurate estimation of the modulation slopes, and of the range through Equation (1). The range measurement accuracy scales as $\Delta d_{acc}/d = \Delta\alpha/\alpha \approx 10^{-3}$.

III. ARCHITECTURE OF THE CHIP

Except from the DFB laser module and output circulators, the LiDAR is fully implemented on-chip. It consists of 8 emission channels and 8 collection channels addressed successively using cascaded Mach-Zehnder switches network and a waveform calibration channel. Thus we avoid beam scanning and the PIC presents no moving parts by having each of the emission part covering the desired angle after passing through collimators. The chip (9 mm^2 of area) designed at Thales Research and Technology (TRT) has been fabricated within IMEC's (Belgium) silicon photonics full platform (ISIPP25G) on 200 mm SOI wafers with 220 nm silicon on a $2 \mu\text{m}$ buried oxide. The PIC was electrically connected to a printed circuit board via wire bondings and the 20 fibers were attached to the grating couplers by Tyndall Institute (Ireland). The functional characterizations and LiDAR experiment were performed by TRT.

Fig. 1 shows the layout of the LiDAR demonstrator. A 75/25 directional coupler at the output of the DFB laser is connected to the chip via grating couplers for the emission part and the delay line interferometer (DLI) (75%). The remaining 25% of the optical power are coupled to the reception part and correspond to the local oscillator.

The delay line interferometer is used to monitor and control the linear chirp of the incident laser. In this interferometer, a 10/90 directional coupler is used to sample the main laser input. A second 10/90 directional coupler splits the light into two branches: the 10% branch goes straight to the output 2×2 combiner, and the 90% branch goes through a 8 cm long (physical length) spiral delay line before reaching the 2×2 combiner. A 170 μm -long thermal phase shifter is also included in one arm of the interferometer to help chirp measurement. Finally, a balanced photodiodes pair (BPD) monitors the output of the interferometer.

A switching network (SN2) routes the laser power (E) to one of the 8 collimation lenses which point in 8 different directions. 8 external fibered optical circulators redirect the collected backscattered light (R) back to the chip on 8 input ports (different

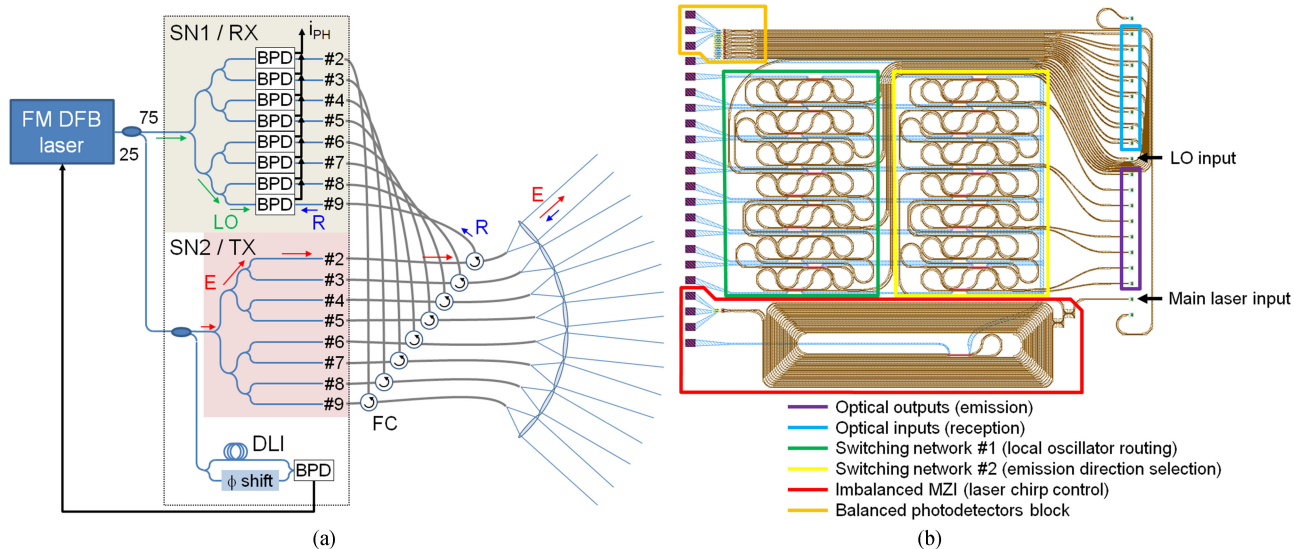


Fig. 1. (a) Architecture of the FMCW LiDAR system. The rectangle delimits the chip perimeter. Switches networks are highlighted in green (SN1) for the reception ports and red (SN2) for the emission ports. Emission channels are successively addressed and connected via optical fibered circulators (FC) to the corresponding Balanced PhotoDiodes (BPD) and the output collimator. The waveform calibration is achieved with the delay line interferometer (DLI). (b) Mask layout of the chip. Metallic pads (purple rectangles on the left) are electrically connected to the printed circuit board and fibers are attached to the grating couplers (blue rectangle on the right). Inset shows a picture of the device.

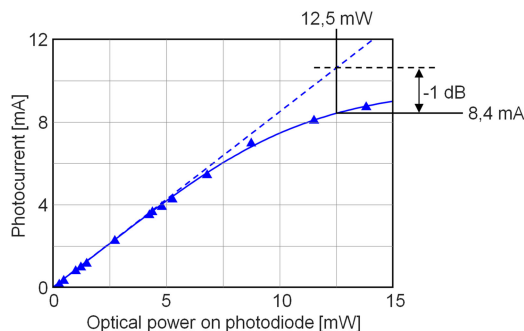


Fig. 2. Photocurrent as a function of the optical power on the photodiode.

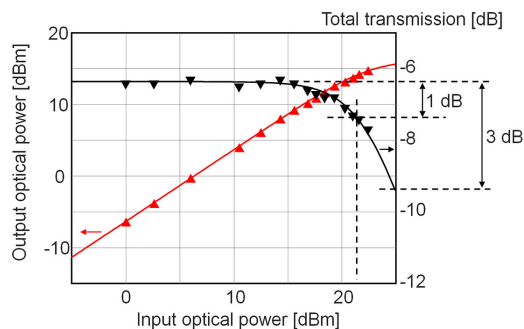


Fig. 3. Shunt waveguide output power (in red, left hand vertical axis) and transmission (in black, right hand vertical axis) versus input optical power.

from the emission ports). In parallel, another switching network (SN1) routes the local oscillator to the balanced photodiodes (BPD) on which the back-reflected signal is incoming. Both switching networks consist in cascaded 2×2 Mach-Zehnder interferometers which are activated by thermal phase shifters (see Fig. 4).

The balanced photodiodes exhibit an efficiency of 0.8 A/W and a -1 dB compression point of 11 dBm (see Fig. 2) and are connected in series. Their summed photocurrents are routed to the RF output. Linearity of the photodiodes with increasing input power is key for heterodyne detection and analogical applications. Both DLI and heterodyne detection RF outputs are sent to a FPGA board. The DLI signal feeds a digital loop which drives the frequency modulated DFB laser, whereas the FMCW LIDAR beating signal is demodulated in the FPGA processing unit and leads to a set of frequency peaks, whose relative positions gives the speed and distance information [4].

The device was packaged and assembled using a specific 20 channels fiber array. Since the fiber length from the chip to circulator has to be kept as small as possible to prevent spurious

interfering signals, the input and output fiber arrays were built using two of the three fiber ports of 8 circulators. The chip to circulator fiber length was thus reduced to 20 cm. The remaining 8 fiber ports of the circulators were connected to the collimation lenses.

For LiDAR applications, the system detection range scales with the emitted power. The power handling of the photonic chip is therefore critical. All the passive waveguides of the circuit were thus designed and fabricated in the 70 nm depth partial etch profile. The optical mode of these shallow-etched waveguides is much less confined than for a deep-etched waveguide, which significantly reduces the nonlinear absorption and allows higher power. However, this also impacts the thermo-optic switches design, where the optical wire waveguides have to be placed further away from the doped silicon striped used for the heaters. Fig. 4 shows on the right hand side the architecture of a Mach-Zehnder switch, where each arm of the Mach-Zehnder is folded twice. The central section of each arm presents then three parallel waveguides, over a length of 120 microns in our case. The left hand part of the figure then shows a cross-section of this

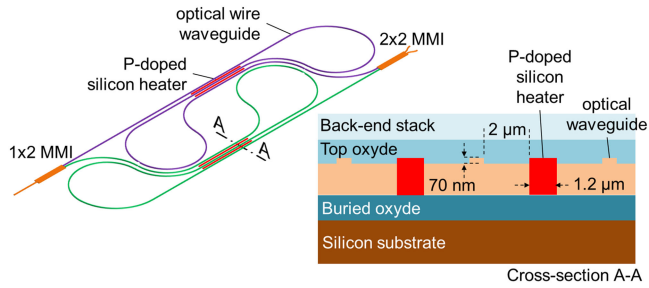


Fig. 4. Left: schematic of a Mach-Zehnder switch cell. The upper and lower arms (respectively in purple and green) are folded around P-doped silicon heaters. Right: cross-section of the heater area.

central zone, where two P-doped, 1.2 μm wide silicon stripes are interleaved between the three waveguides. To avoid additional propagation loss, the spacing between the waveguide and the heaters is 2 microns, to be compared to 600 nm for deep etched waveguides [15]. The thermal phase shifters were therefore less efficient, with 40 mW of electrical power required for a 2π phase shift, against 20 mW for their deep etched counterparts.

A shunt waveguide was used to measure the output optical power as a function of the input power, to determine the input power levels for 1 dB and 3 dB additional losses (respectively 1 dB and 3 dB compression power levels). From Fig. 3, the insertion losses are -6.4 dB in the low power regime, and increase to -7.4 dB for 22 dBm optical input power (19 dBm at waveguide input). Extrapolating the measured data, we can estimate that insertion loss would further increase to -9.4 dB (-3 dB additional loss) for an optical power of 25 dBm (so 22 dBm at waveguide input).

The emission switch network was calibrated by maximizing the output optical power as a function of the electrical power applied to the heaters. The crosstalk, estimated by comparing the optical power in the routed channel to the optical power in the other channels lead to a channel isolation higher than 30 dB. The 1 to 8 switching networks induce 2.3 dB of losses. Similarly, the reception switch network was calibrated by successively sending a frequency shifted optical signal at each of the 8 receiver inputs. The receiver switch voltage controls are then adjusted to route the local oscillator to the selected detector, hence maximizing the heterodyne beatnote at the balanced receiver.

IV. RANGING EXPERIMENT

Apart from the thermal drift issues mentioned in Section II, the length of the delay line in the chirp calibration DLI is also critical to reach good precision. In Fig. 5, the FFTs of the demodulated signal are plotted for each slope and for different lengths of the delay line used to calibrate the frequency modulated waveform. Basically, the shorter the delay line, the larger the error on the FM waveform optimization, and therefore the demodulation error. In particular, a doubling of the peaks is observed for the on-chip delay line of 8 cm (1 ns delay), which decreases the measurement accuracy. On the right part of the figure, the signal with an external delay line of 5 m (24 ns delay) shows better definition of the peaks and error free

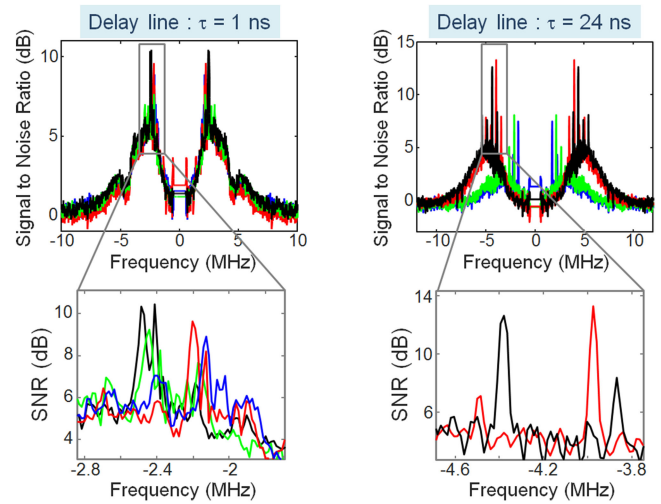


Fig. 5. Illustration of the detection peaks degradation with the length of the calibration delay line. On the left hand side, the 1 ns integrated delay line leads to peak doubling, whereas with a 24 ns external fiber delay line, the peaks are perfectly resolved.

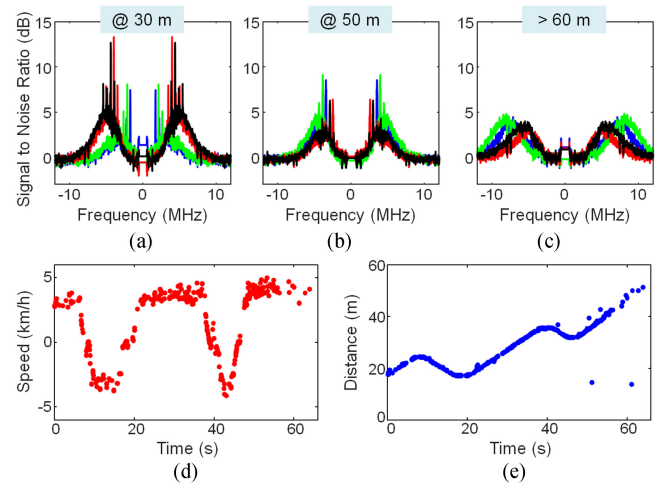


Fig. 6. Speed and range measurement at up to 60 m range with only 5 mW of emitted laser power. The external delay line of 24 ns is used. FFT spectra for increasing ranges are displayed (a to c) and the measured speed and range are shown in d and e.

signal processing. Longer delay lines could be implemented easily considering the signal level collected at the delay line interferometer photodiodes.

In order to increase the detection range, we use the external 5 m fibered delay line during the first experiment. The experiment whose results are plotted in Fig. 6 takes place outdoors on a clear day, i.e., with excellent visibility. A pedestrian is walking in front of the optical head back and forth at a normal speed. The pedestrian's path is contained within the field of view of a single collimator. Range and speed in Fig. 6(e) and 6(d) are thus obtained for a given configuration of the switch networks. With an emitted optical power of 5 mW, we are able to demonstrate speed and range measurement at up to 60 m. The FFT spectra plotted in Fig. 6(a), shows the back-reflected signal for a target walking at 30 m with a speed of 5 km/h. The signal to noise ratio is 15 dB but a pedestal related to the coherence length of the

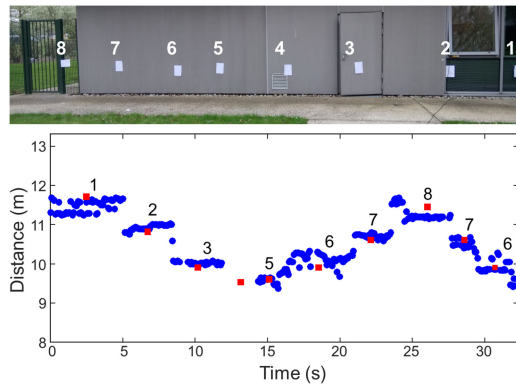


Fig. 7. Scanning of a wall at a distance of 9.5 meters with the 8 scanning directions. Top : Picture of the wall, white paper sheets indicate the location of the laser spots during scanning. Bottom : The processed distances of the successively switched directions are plotted (blue dots). Red squares indicate the calculated distance to the wall under the successive scanning angle.

DFB laser goes up to 5 dB. Fig. 6(b), shows similar spectra for a target at 50 m with a negative speed -5 km/h. Though the SNR is smaller than at 30 meters, it is still 5 dB above the pedestal and enables the peaks processing. Over 60 meters (Fig. 6(c)), the relevant peaks are still visible with a comfortable signal to noise ratio, but a larger noise pedestal around the peaks strongly reduces the accuracy and resolution. Similar experiment was carried out with the on-chip delay line of 1 ns for the waveform calibration but, for ranges above 30 m, the noise pedestal was detrimental for accuracy. Measurements of higher speed are perfectly feasible provided the Doppler shift remains below the half-bandwidth of the ADC ($v_{\pm} < BW_{DAC}/2$). Furthermore, from Equations (1) and (2), the laser chirp α , and the speed and range of the target are linked by $2\alpha d/c + 2v/\lambda = v_{\pm}$. This sets the application scenario of the system. As an example, with our chirp waveform, the detection of a target with a radial velocity of 300 km/h at 100 m would require an ADC with a minimum bandwidth of 250 MHz.

We also assessed the proper operation of the 8 LiDAR channels by pointing at a wall at 9.5 meters. The 8 directions, covering a total angle of 70° are successively selected. The experimental conditions were 5 mW of output power and the on-chip delay line (1 ns) was used to calibrate the waveform. In Fig. 7, the experimental range varies as a function of the incidence angle on the wall from 11.5 meters for the outmost directions (#1 and #8) down to 9.5 meters for the central direction #5. Clear steps are spotted when directions are successively selected. On the picture, we show with paper sheets the area of the spots, although these are not necessary to reflect light (except for spots #1 and #2 on the windows). Spot #4 is not measured because the demodulated peaks at such a short distance fall into the stopband of a numerical low pass filter in the processing step. This filter of 0.6 MHz width enables to remove any peak caused by the reflection at the output imaging system. Red squares show the distances derived from the scanning angle and the normal distance to the wall. The experimental measurements hence show excellent agreement with the scene configuration.

V. CONCLUSION

In this paper, we have performed detection and ranging of a moving target at up to 60 m with less than 5 mW of output power with a fully CMOS-compatible photonic integrated circuit. Apart from the DFB laser and circulators, the optical part of the LiDAR was comprised in a 9 mm^2 chip. We demonstrated up to 20 mW of output power for 200 mW input power and a homogeneous routing over the 8 channels. In these experiments, detection was not limited by the optical output power but rather by the noise of the modulated DFB laser. The length of the on-chip delay line of the DLI, critical for the calibration of the waveform was also an issue for accurate measurements over 30 m. Other calibration schemes may be studied such as IQ demodulation [16] in order to overcome the limitation of the length of the delay line.

Detection and ranging on-chip using integrated photonics should definitely offer compactness and reduce costs but for longer ranges or wind measurements, the high power sustainability of the chip should be improved.

REFERENCES

- [1] A. Dolfi-Bouteyre, G. Canat, L. Lombard, M. Valla, A. Durécu, and C. Besson, "Long-range wind monitoring in real time with optimized coherent lidar," *Opt. Eng.*, vol. 56, no. 3, pp. 031 217–031 217, 2017.
- [2] C. Weitkamp, *Lidar: Range-Resolved Optical Remote Sensing of the Atmosphere*, vol. 102. New York, NY, USA: Springer, 2006.
- [3] P. Feneyrou *et al.*, "Frequency-modulated multifunction lidar for anemometry, range finding and velocimetry—2.experimental results," *Appl. Opt.*, vol. 2, no. 57, pp. 9676–9685, 2018.
- [4] P. Feneyrou *et al.*, "Frequency-modulated multifunction lidar for anemometry, range finding and velocimetry—1.theory and signal processing," *Appl. Opt.*, vol. 2, no. 57, pp. 9663–9675, 2018.
- [5] A. M. Pawlikowska, A. Halimi, R. A. Lamb, and G. S. Buller, "Single-photon three-dimensional imaging at up to 10 kilometers range," *Opt. Express*, vol. 25, no. 10, pp. 11 919–11 931, May 2017. [Online]. Available: <http://www.opticsexpress.org/abstract.cfm?URI=oe-25-10-11919>
- [6] I. Coddington, W. C. Swann, L. Nenadovic, and N. R. Newbury, "Rapid and precise absolute distance measurements at long range," *Nature Photon.*, vol. 3, no. 6, pp. 351–356, 2009.
- [7] C. Weimann *et al.*, "Measurement of length and position with frequency combs," in *J. Phys. Conf. Ser.*, vol. 605, no. 1, 2015, Art. no. 012030.
- [8] P. Trocha *et al.*, "Ultrafast optical ranging using microresonator soliton frequency combs," *Science*, vol. 359, no. 6378, pp. 887–891, 2018.
- [9] M.-G. Suh and K. Vahala, "Soliton microcomb range measurement," *Science*, vol. 359, no. 6378, pp. 884–887, 2018.
- [10] F. Aflatouni, B. Abiri, A. Rekh, and A. Hajimiri, "Nanophotonic coherent imager," *Opt. Express*, vol. 23, no. 4, pp. 5117–5125, 2015.
- [11] B. Behroozpour *et al.*, "Electronic-photonic integrated circuit for 3-D microimaging," *IEEE J. Solid, State Circuits*, vol. 52, no. 1, pp. 161–172, 2017.
- [12] C. V. Poulton *et al.*, "Coherent solid-state lidar with silicon photonic optical phased arrays," *Opt. Lett.*, vol. 42, no. 20, pp. 4091–4094, 2017.
- [13] Z. Du, G. Luo, Y. An, and J. Li, "Dynamic spectral characteristics measurement of DFB interband cascade laser under injection current tuning," *Appl. Phys. Lett.*, vol. 109, no. 1, 2016, Art. no. 011903. [Online]. Available: <https://doi.org/10.1063/1.4955411>
- [14] T. DiLazaro and G. Nehmetallah, "Multi-terahertz frequency sweeps for high-resolution, frequency-modulated continuous wave lidar using a distributed feedback laser array," *Opt. Express*, vol. 25, no. 3, pp. 2327–2340, 2017.
- [15] C. Scarcella *et al.*, "Plat4m: Progressing silicon photonics in Europe," *Photonics*, vol. 3, no. 1, pp. 1–10, 2016.
- [16] P. Feneyrou, G. Pillet, and J. Minet, "Method for generating m demodulation signals," Patent EP20150165519, Nov. 4, 2015. [Online]. Available: <https://www.google.com/patents/EP2940522A1?cl=en>

Aude Martin received the Ph.D. degree in nonlinear optics from Universit Paris Saclay, Paris, France.

She has gained expertise in fabrication of photonic integrated circuits and led theoretical and experimental analysis of extreme nonlinearities in photonic nanostructures. She is currently involved with the development of fibered and photonic integrated LiDAR systems, Thales Research and Technology, Palaiseau, France.

Delphin Dodane received two Master's degrees: one in microelectronics from Institut National Polytechnique de Grenoble, Grenoble, France, and other in fundamental optics from Université Paris-Saclay, Paris, France, in 2016 and 2017, respectively. He is currently working toward the Ph.D. degree at Thales Research and Technology, Palaiseau, France.

His research interests include microwave photonics and photonic integrated circuits.

Luc Leviandier received the Graduate's degree from Ecole Nationale Supérieure de Physique de Grenoble, Grenoble, France, and Université Joseph Fourier de Grenoble, Grenoble, France.

In 1986, he as a Research Engineer joined Thales (formerly Thomson-CSF). Between 2000 and 2009, he was a Associated Professor with Université du Maine. Since 2008, he is with the Physics Research Group, Thales Research and Technology. He has been responsible of theoretical and numerical studies on wave propagation, wave scattering and signal processing of acoustic, and electromagnetic and optical waves for applications to design and performance assessment of sonar, radar, and more recently LiDAR systems.

Daniel Dolfi (SM'17) received the Graduate degree from the Ecole Supérieure d'Optique, Orsay, France, 1986, the Ph.D. degree from University Paris XI Orsay, Orsay, France, in 1993, and the Habilitation Diriger des Recherches, in 2008.

In 1986, he joined Thomson-CSF Corporate Research Laboratory (now Thales Research and Technology-France), where he is currently the Director with the Department of Physics. He has authored or co-authored more than 80 publications in refereed journals and 130 communications in international conferences and holds 70 registered patents. His main research interests include optoelectronic generation and processing of microwave and THz signals, nonlinear optics in fibers, opto-electronic devices (down to nanoscale) and sub-systems (e.g., sensors), active optronic systems (lidars and imaging systems), superconductor based microwave devices, and graphene based optoelectronics.

Dr. Dolfi is an EOS Fellow and an OSA Fellow.

Alan Naughton received the B.Sc. degree in applied physics and electronics from the National University of Ireland, Galway, Ireland, in 2007, and the Ph.D. degree in physics from Tyndall National Institute, Cork, Ireland, and University College Cork, Cork, in 2014, respectively. His Ph.D. research was focused on next-generation optical access networks.

In January 2016, he was a Research Scientist with the Photonics Packaging Group, Tyndall National Institute, where he continued his research in the Photonics Systems Group. His role involves the management of photonic packaging activities in a wide range of research projects along with associated research activities in photonic and electronic packaging and integration.

Peter O'Brien received the Graduate and Ph.D. degrees in physics from Trinity College Dublin and University College Cork, Cork, Ireland, respectively.

He previously founded and was the CEO of a start-up company manufacturing speciality photonic systems for bioimaging and pharmaceutical product monitoring applications, which he sold in 2009. Prior to this, he was a Post-doctoral Scholar with the California Institute of Technology, Pasadena, and a Research Scientist with NASA's Jet Propulsion Laboratory, where he was involved in the development of submillimetre wave devices for remote (space) sensing applications. He is the Director of the European Photonics Packaging Pilot Line and the Head of the Photonics Packaging Group, Tyndall Institute, University College Cork, Ireland. He is also a Lead Partner with the PIC Device Pilot Line, and a Board Member of JEPPIX and ePIXfab, InP and Si photonic device foundry services, respectively. His group develops photonic microsystems for high-speed fiber optic communication, medical devices, and sensing applications. He is also an Adjunct Professor with the College of Optical Sciences, the University of Arizona, Tucson, AZ, USA.

Thijs Spuessens, biography not available at the time of publication.

Roel Baets, biography not available at the time of publication.

Guy Lepage, biography not available at the time of publication.

Peter Verheyen, biography not available at the time of publication.

Peter De Heyn, biography not available at the time of publication.

Philippe Absil received the Ph.D. degree from the Department of Electrical Engineering, the University of Maryland, College Park, MD, USA, in 2000.

Since 2013, he has been the Director of the Department of 3-D and optical I/O technologies, IMEC, and since 2010, has been responsible for the silicon photonics technology platform development. Before that he was with IMEC for seven years managing the advanced CMOS scaling program. In the early 2000s, he developed the passive photonics platform technology for Little Optics, Inc., Maryland, USA. His doctoral work contributed to the early demonstrations of semiconductor microring resonators.

Patrick Feneyrou received the Ph.D. degree in nonlinear spectroscopy.

Since 1998, he is with the Thales Research and Technology, Palaiseau, France. Since 2003, he is in charge of the theoretical analysis, system simulation, and development of proof of concept of LiDAR systems. He has developed several LiDAR systems for laser anemometry, temperature sensing, range finding, and velocimetry.

Jérôme Bourderionnet received the Ph.D. degree in laser physics.

Since 2001, he has been working with the Department of Physics, Thales Research and Technology, Palaiseau, France. His research interests include microwave photonics for signal processing, and photonic integrated circuits.